Joint Inversion of the Differential Satellite Interferometry and GPS Data: a Case Study of Altai (Chuia) Earthquake of September 27, 2003

V. O. Mikhailov[a], A. N. Nazaryan[a], V. B. Smirnov[a,b], M. Diament[c], N. Shapiro[c], E. A. Kiseleva[a], S. A. Tikhotskii[a], S. A. Polyakov[b], E. I. Smol'yaninova[a], and E. P. Timoshkina[a]

[a] *Schmidt Institute of Physics of the Earth, Russian Academy of Sciences, Bol'shaya Gruzinskaya ul. 10, Moscow, 123995 Russia*
e-mail:mikh@ifz.ru
[b] *Faculty of Physics, Moscow State University, Moscow, 119991 Russia*
[c] *Institut de physique du Globe de Paris (IPGP), France*
Received September 09, 2009

Abstract—Based on the data of differential satellite interferometry, the field of displacements of the Earth's surface in the line-of-sight direction is determined for the region of the Altai Earthquake that struck on September 27, 2003. The displacements are estimated for unforested areas of Chuia and the Kurai depressions, and for a part of their mountainous surroundings. In that part of the region where unwrapping of the data was possible, the amplitude of displacements amounts up to 150 cm for Chuia and 100 cm for the Kurai depressions. In order to locate the surface of the seismic rupture and to find the field of displacements on this surface, the method for the combined inversion of the displacements data, provided by satellite interferometry (the present work) and geodesy [Gol'din et al., 2005], is suggested and applied. The admissible range of the parameters of the rupture was specified from the seismology and seismotectonics data.

The combined use of geodetic and satellite interferometry data makes the solution of the inverse problem more stable and yields a seismic momentum estimate, which is consistent with the seismological determinations. We discuss the possible contributions of various postseismic processes; in particular, based on analyzing the energy of the aftershocks, we assess the contribution of the postseismic creep to the displacements, determined from the interferometry and geodesy data, for different coseismic and postseismic time intervals.

The combined use of geodetic and satellite interferometry data makes the solution of the inverse problem more stable and yields a seismic momentum estimate, which is consistent with the seismological determinations. We discuss the possible contributions of various postseismic processes; in particular, based on analyzing the energy of the aftershocks, we assess the contribution of the postseismic creep to the displacements, determined from the interferometry and geodesy data, for different coseismic and postseismic time intervals.

INTRODUCTION

Owing to the advances in the GPS and GLONASS global positioning systems and in the interferometric synthetic aperture radars (InSAR), in the past decade, it became possible to obtain detailed data about the displacements of the Earth's surface in the focal regions of a series of earthquakes. These data were used as a basis for the detailed study of deformations of the Earth's crust in the focal zones of earthquakes; the methods for reconstructing the geometry of the rupture and the field of dislocations along the rupture were developed; the mechan-

ics of the lithosphere in different coseismic and postseismic processes was investigated [Massonet et al., 1993; Hudnut et al., 1994; Freymueller et al., 1994; Peltzer et al., 1998; Fialko et al. 2001; Simons et al. 2002; Johnson et al., 2002; and many other works].

With the use of the global positioning system, it is possible to measure the horizontal (northward and eastward) and vertical components of the displacements (the latter is usually estimated with much lower accuracy). From the data provided by the satellite interferometry, it is possible to find the line-of-sight (LOS) projection of the full vector of displacement of a certain element on the Earth's surface that corresponds to a pixel in the radar image, which results in the selective sensitivity of the InSAR data. On the other hand, satellite interferometry in many cases provides a more detailed and complete coverage of the target region, in contrast to geodetic measurements, which are usually carried out at a limited number of observation sites. An exception is the GEO-NET system (GPS Earth observation network of Japan) [Tsuda et al., 1998] and the South California integrated GPS Network (SCIGN), where an exceptionally dense coverage is achieved.

Geodetic determinations can be carried out with a short period of repeatability, especially at the base stations. The minimum interval for obtaining the repeat-pass interferometric image for ENVISAT, ERS-1,and ERS-2 satellites is 35 days (except for a short period of simultaneous tandem-mode orbital operation of the two latter satellites). Hence, geodetic and interferometric data in fact are mutually supplementary and should thus be interpreted in common.

This work concerns the analysis of coseismic and postseismic deformations in the region of the Altai (Chuia) earthquake of September 27, 2003. This earthquake is rather well studied by ground and satellite methods and is the topic of many publications including [Nissen et al., 2007; Barbot et al., 2008], where the data of the differential satellite interferometry (DInSAR) are analyzed. In our paper, we use not only the interferometric but also the geodetic data. Geodetic measurements in Altai were taken in 2000 by scientists of the Institute of Oil Geology and Geophysics of the Siberian Branch of the Russian Academy of Sciences. These works were leaded by Academician S.V. Gol'din, and the results of 2003–2004 were published in [Gol'din et al., 2005]. Unfortunately, the data of later measurements, as far as we are aware, have not been published. For the purposes of a combined interpretation, we developed a specialized inversion technique, allowing for particular features of the geodetic and interferometric data available. In our work, we also estimate the error that results from the fact that the interferometric and geodetic measurements refer to different time intervals.

The first part of the paper presents a brief outline of the Altai earthquake, which will be necessary for the formulation of the problem and the interpretation of data. Then, we describe the procedures of processing the InSAR data and obtaining the estimations for the field of the LOS displacements of the ground. After this, we consider the methods for the joint inversion of the geodetic and interferometric data and discuss the results and their interpretation. Note that the available geodetic data are not sufficiently detailed to allow the determination of the geometry of the rupture and the field of displacements along the rupture. However, the inclusion of geodetic data brought about considerable changes in the models yielded by the satellite interferometry alone [Nissen et al., 2007; Barbot et al., 2008].

## ALTAI (CHUIA) EARTHQUAKE OF SEPTEMBER 27, 2003

Numerous data show that the collision of Indian and Eurasian plates produces the stresses and deformations in a large zone, extending more than 2500 km northwards and overlapping South Siberia, including the Altai and Sayan. According to years-long GPS measurements, the rate of convergence between these plates is 35 mm per year, and up to 20% of the common approach of the plates occurs in Altai, where the horizontal shortening reaches 7 mm per year [Calais et al., 2003]. The general pattern of motions in this region is rather complex (see, e.g., [Timofeev et al, 2006]), which is due, in particular, to the fact that the lithosphere at that region is highly heterogeneous in its structure and thermal conditions. In addition to the collision of the Indian and Eurasian plates, another factor that determines the kinematics in the Mountain Altai is the uplift and radial extension due to the warm, buoyant Hangay Dome [Cunningham, 2005], and the splitting of the tectonic flow in the South Mountain Altai into the northwest and northeast branches [Gol'din et al., 2005]. The region of the Altai earthquake of September 27, 2003 is located on the northwest branch, close to the point of divergence of the tectonic flows.

With a view to studying the fields of surface displacements in the region, the Altai geodynamical testing area was laid in 2000 by a team from the Institute of Oil Geology and Geophysics of the Siberian Branch of the Russian Academy of Sciences, lead by Academician S.V. Gol'din. This testing area extends from Novosibirsk to the Mongolian border; in 2003, there were 20 points of repeated observations and one base station installed there [Timofeev et al., 2006]. The measurements of 2003–2004 detected the displacements caused by the Altai earthquake (Fig. 1), which amounted to more than 30 cm at the observation points close to the focal zone of the earthquake [Gol'din et al., 2005].

The main seismic event occurred on September 27, 2003 at 11:33:24.94 Greenwich mean time. The coordinates of its epicenter were 49.97°N, 87.77°E, according to the refined data of the Information and Processing Center of the Geophysical Service of the Russian Academy of Sciences (IPC GS RAS) and the European–Mediterranean Seismological Centre (EMSC). The focal depth was estimated by different seismological centers as 16–18 km; the magnitude of the main shock was 7.0–7.3, in accordance with different data sources; and the intensity of vibrations in the epicenter reached 9. The main seismic event was followed by numerous aftershocks. Two large events were 6.2 and 6.6 in magnitude and hit the region on the day of the main event at 18:53 Greenwich mean time and on October 01, 2003 at 01:03 at the northwestern extension of the main rupture [Starovoit et al., 2003; NEIC data]. Analyzing the seismograms, E. Nissen with colleagues [2007] identified one more seismic event, which occurred presumably southeastwards of the epicenter of the main event 10 seconds after it; the magnitude of this event was 6.7 (Fig. 1). Discrimination of events, so close in time, in the seismograms is a very difficult task, therefore, it is essential that the above inference is confirmed by the seismotectonical observations and satellite interferometry data.

The tectonic rupture on the surface of sedimentary cover has been discovered on the southern slopes of the Chuia and Kurai depressions, in the zone of their junction with the North and South Chuia Ranges (Fig. 1). It was possible to trace several segments of the rupture as far as 50 km away [Geodakov et al., 2003; Nissen et al., 2007]. According to [Delvaux et al., 1995], the Chuia
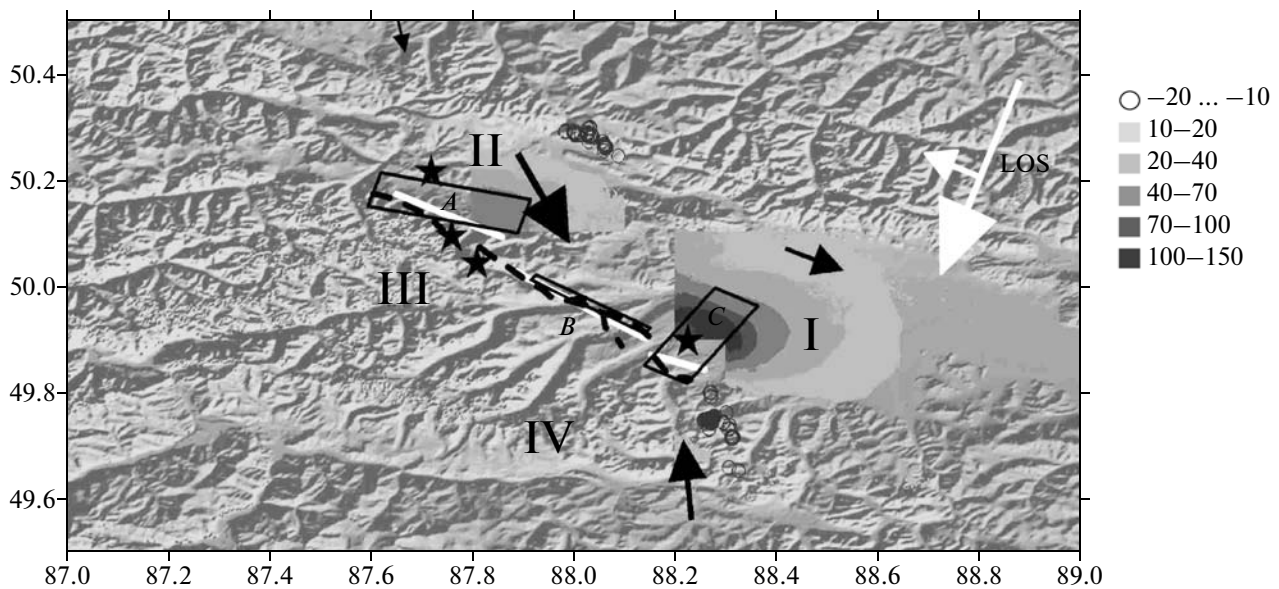
Fig. 1. The field of the displacements in the line-of-sight direction, obtained from the pair of images 2—7 for the Chuia (indicated by the numeral I) and 1-4 for the Kurai (indicated by the numeral II) depressions (Table 1). The displacements towards the satellite are shown by shades of grey; the displacements in the opposite direction are shown by circles. The ground projection of the rupture's surface in the model by [Nissen et al., 2007] is shown by the white lines; the positions of the surface rupture from that same work are shown by the dashed black line. The projections of the planes approximating the rupture, which were obtained in our work, are shown by black squares. The asterisks indicate the main event (northwards of the plane *B*), the two main aftershocks (in the region of plane *A*) in accordance with the IPC GS RAS data [Starovoit et al., 2003], and the aftershock in the area of the plane *C*, determined in the work [Nissen et al., 2007]. The large white arrow in the upper right-hand corner is the direction of the satellite motion; the smaller arrow perpendicular to it indicates the line-of-sight direction. The black arrows are the horizontal displacements, in accordance with the GPS data [Gol'din et al., 2005]; III and IV are the North and South Chuia Ranges.

depression, filled with the sedimentary Cenozoic rocks, was raised as a result of the extension in the Oligocene—Early Pliocene. The compression and inversion started in the Late Pliocene along this same fault system, which remains active up to date.

Numerous aftershocks are distributed within a wide area about the rupture surface. Lutikov with colleagues [2003] found a gradual propagation of the aftershock activity to the northwest of the epicenter of the main event. The advancement of the rupture lasted a few days and stopped soon after a strong aftershock struck on October 1, 2003; therefore, it is particularly difficult to discriminate between the coseismic and postseismic events in this case.

ESTIMATION OF THE GROUND DISPLACEMENTS BY DIFFERENTIAL SAR INTERFEROMETRY

At present, there are a series of satellites orbiting in space, which are surveying the Earth's surface with the use of synthetic aperture radars, operating in different frequency bands and, thus, providing different spatial resolution of measurements. The data of the radio location (often called images) are usually represented in the form of a two-dimensional matrix of complex readings, each being characterized by its amplitude and phase. The coordinates of matrix elements are the azimuth (the

direction along the satellite path) and the slant range (the distance across the satellite path). If, for the same element of the Earth's surface, there are two radiometric images available, measured from two locally parallel orbits that are close to each other, it is possible to find the LOS displacement of this surface element [Hanssen, 2001]. Based on these two images, a complex interferogram is calculated, each element of which is a product of the backscattered signal of the first image and the complex conjugate signal of the second image. The phase of each element in this interferogram is the phase difference of these two images. The phase difference is proportional to the difference in the distances to the reflecting element of the Earth's surface, but it depends also on both the topography and the geometry of the survey, and on the atmospheric and atmospheric delays as well.

In the same way as the geodetic measurements, the satellite interferometry data contain errors caused mainly by the ionospheric and atmospheric influence. Ionospheric effects often appear as a linear trend persistent through the whole interferogram; in this case, they are easily recognizable and can readily be eliminated [Samsonov et al., 2008]. The most difficult problem is how to dispose of the water vapor effect in the atmosphere. In particular, it is shown in [Hanssen and Feijt, 1996] that variations in temperature, density, and water content in the air may result in false LOS displacements that are as large as a few centimeters, calculated from the satellite

Table 1. ENVISAT satellite images used in the analysis of the Altai earthquake of September 27, 2003

Number	Date	Orbit	Track
1	August 23, 2003	7731	162
2	September 8, 2003	7960	391
3	September 11, 2003	8003	434
4	October 13, 2003	8461	391
5	October 16, 2003	8504	434
6	December 6, 2003	9234	162
7	December 22, 2003	9463	391
8	December 25, 2003	9506	434
9	July 19, 2004	12469	391
10	July 22, 2004	12512	434

interferometry data. Such effects manifest themselves as separate spots related with large clouds, or as vast regions, corresponding to the atmospheric fronts [Hanssen, 2001; Massonnet and Feigl, 1998]. Several approaches are suggested for reducing these errors, including those involving the data from other spacecrafts.

In order to estimate the surface displacements in the region of the Altai earthquake, we used ten images from the ENVISAT satellite of the European Space Agency (Table 1). The criterions for image selection were (a) the maximum possible coverage of the target territory; (b) the length of the baseline (the distance between satellite positions corresponding to the first and second images) not exceeding 600 m; (c) close Doppler frequency shifts for the pair of images; and (d) favorable seasonal and climate conditions. The initial size of the image is 100×100 km, the spatial resolution is about 30 m, and the polarization during the survey is vertical.

Interferometric processing of the satellite data was executed using the ROI_PAC software (Repeat Orbit Interferometry PACkage), developed in the Jet Propulsion Laboratory, California Institute of Technology. The digital model of the target region's topography, which is required for processing the data, is constructed from the data of topographic surveying carried out during the Shuttle Radar Topography Mission (SRTM). The rest of the data necessary for the interferometric image processing are taken from the open database of the Delft University of Technology (DEOS).

The processing of seven interferometric pairs of images provided the phase interferograms, displaying the phase shifts of the signal, reflected from each surface element during the time interval between the images. The phase shift is measured in radians and varies within $(-\pi, \pi)$. The phase interferograms were transformed into the LOS displacement field via phase unwrapping executed in accordance with two algorithms, GZW [Goldshtein et al., 1988] and SNAPHU [Goldshtein et al., 1993]. The results yielded by the SNAPHU algorithm for the Altai region proved less dependent on the coherence of images used in the interferogram calculation. These

results provided a more dense coverage of the target region and showed better consistency with the earlier results [Nissen et al., 2007; Barbot et al., 2008]. The detailed description of data processing can be found in [Nazaryan, 2008].

Figure 1 depicts the LOS displacements obtained by the superposition of the results of phase unwrapping for the pair 1—4 for the Kurai depression and the pair 2—7 for the Chuia depression (Table 1). The differential interferogram was converted into LOS displacements. These displacements are displayed in shades of grey against the volumetric background topography. The small region of negative values is shown by circles clustering on the mountain slopes southwards of the Chuia and northwards of the Kurai depressions. It proved possible to build the interferograms for a few pairs of images; reconstruction of the displacement fields from different pairs of images yielded close to similar results. A distinct interferometric pattern is obtained for the unforested areas with relatively smooth topography, namely, for the Kurai and Chuia depressions and for a part of their mountainous surroundings. The loss in correlation is mostly due to the mountain topography and high-density of forest vegetation on the mountain slopes.

The black dashed line in Fig. 1 outlines the position of the rupture on the surface of the sedimentary cover, in accordance with the data in [Geodakov et al., 2003; Nissen et al. 2007]. The black squares show the ground projection of our model; the white lines correspond to the position of the upper boundary of the model [Nissen et al., 2007]. The black arrows are the vectors of relative displacements, according to GPS data [Gol'din et al., 2005], in the closest region to the rupture in 2003—2004. The white arrows in the right-hand upper corner indicate the direction of satellite motion and the direction of the survey.

It is impossible to digitize the entire interferogram in the vicinity of the rupture because of the severe deformations in this region. The amplitude of the uplift in the region of the Chuia depression exceeds 1.5 m in our digitization (against 1.9 m in the work [Nissen et al., 2007])

and in the region of the Kurai depression, about 1 m. These displacements are produced by the main seismic event and by extremely strong aftershocks (on September 27 and October 1, 2003) as well as by the postseismic processes that lasted up to October 13, 2003 in the Chuia depression, and December 22, 2003 in the Kurai depression. It is important that the geodetic data characterize these same events and the postseismic processes as well, but for periods extending up to May and July, 2004, inclusive [Gol'din et al., 2005]. In the following section of the paper, we will determine the geometry of the rupture surface and find the field of displacements along this surface, assuming that the ground displacements result mainly from the rock motion along the main rupture and its northwest and southeast extensions. After doing this, we will turn back to the assessment of the possible contributions of the postseismic processes. In particular, we will estimate the error caused by the fact that the geodetic data span a longer time interval than the interferometry.

DETERMINATION OF THE FIELD OF DISPLACEMENTS ON THE RUPTURE: THE STATEMENT OF THE PROBLEM

The mathematical description of short-period deformations in the Earth's crust, which are caused by low-magnitude earthquakes, often relies on the model of elastic half-space with a cut that reproduces the seismic rupture. If the rupture is approximated by the set of planes, we can use the analytical solution for the fields of stress and deformation from each plane (see, e.g., [Okada, 1985]). In the scope of the linear theory of elasticity, the entire displacement on the surface is a sum of the displacements from all planes.

Each plane is characterized by nine parameters: three coordinates, e.g., of some of its corners; the strike and the dip lengths; the strike and the dip angles; and two components of the displacement vector. It is important that some of these parameters can be determined a priori and then used as the initial guess in the inverse problem solution. Indeed, in order to estimate the average dip and strike angles of the rupture, we may choose such a nodal plane that agrees with the position of the seismic rupture on the surface of sedimentary cover, which is mapped by the seismotectonic survey in the Altai (Fig. 1). This allows us to construct a more adequate model of the rupture that consists of a few planes, and to estimate the extension of each of the planes. Because the shape of the rupture on the surface of the sedimentary cover is always more complex than its configuration in the underlying crystalline basement, the surface trace of the rupture is usually smoothened. This also enables reducing the contributions of the second-order processes such as landslides, topography effects, heterogeneities in the physical properties, and variations in the thickness of the sedimentary cover. The main difficulty is to estimate the dip, strike, and the depth of the upper and bottom edges for each plane, and to determine the components of the displacement vector, which are parallel to the dip (U_n) and strike (U_{SS}) of the rupture.

The problem was stated as follows. Let the interferometric data on the LOS displacements, $W_{\text{LOS}}(\varphi_i, \lambda_i)$, be known for the region of the earthquake. Let also the GPS data that characterizes the northward and eastward coseismic displacements, $\{V_{\text{north}}(\varphi_j, \lambda_j), V_{\text{east}}(\varphi_j, \lambda_j)\}$, be available at several points of repeated observations. We approximate the rupture by a set of planes, and use the solution of the problem of plane dislocation in the elastic half-space for the description of the field of displacements on the Earth's surface [Okada, 1985]. Within each plane the components of the displacement in the dip and strike directions, U_n^i and U_{SS}^i, are assumed to be constant; they should be determined in the inverse problem solution which reduces to the minimization of the selected misfit functional over the interferometric and geodetic data.

The strategy for the solution of the problem is as follows. The rupture is approximated by a set of planes. The parameters of the planes and the components of the displacement vectors are found from the best fit of the measured to the calculated data. The algorithm implies successive partitioning of each plane into four equal subregions, then into eight, and so on (each subregion with the same dip and strike as the initial plane), until a stable solution and misfit are attained. Such a scheme provides sufficient detail of the solution, but allows avoiding its oversegmentation, which may lead to instabilities. The solution is sought for by the minimization of the functional

$$
\begin{aligned}
\Phi_\beta(\mathbf{p}) = &\left\| V_{\text{east}}^{\text{meas}} - V_{\text{east}}^{\text{calc}}(\mathbf{p}) \right\|_{L_2}^2 \\
+ &\left\| V_{\text{north}}^{\text{meas}} - V_{\text{north}}^{\text{calc}}(\boldsymbol{p}) \right\|_{L_2}^2 + \alpha \left\| W_{\text{LOS}}^{\text{meas}} - W_{\text{LOS}}^{\text{calc}}(\boldsymbol{p}) \right\|_{L_2}^2 \\
+ &\beta \{ \left\| \partial^2 U_{SS}^i/\partial x^2 \right\|_{L_2}^2 + \left\| \partial^2 U_n^i/\partial x^2 \right\|_{L_2}^2 \\
+ &\left\| \partial^2 U_{SS}^i/\partial y^2 \right\|_{L_2}^2 + \left\| \partial^2 U_n^i/\partial y^2 \right\|_{L_2}^2 \},
\end{aligned}
\tag{1}
$$

where the calculated displacements in the GPS observation points ($V_{\text{north}}^{\text{calc}}$, $V_{\text{east}}^{\text{calc}}$) and in the grid points, where the displacements are specified in accordance with interferometry data ($W_{\text{LOS}}^{\text{calc}}$), depend on the vector of parameters $\mathbf{p} = (\mathbf{u}; \mathbf{g})$. Here, $\mathbf{u} = (u_n^1, ..., u_n^N; u_{SS}^1, ..., u_{SS}^N)$ is the vector of unknown displacements at each element of the initial plane partition in the dip (u_n^i) and strike (u_{SS}^i) directions; N is the total number of partition elements (discretes); $\mathbf{g} = (g_1, ..., g_M)$ is the vector of parameters, which define the positions of the planes approximating the rupture. It is important that the surface displacements linearly depend on the components of $\mathbf{u}$, and nonlinearly, on $\mathbf{g}$. The second derivatives in the curly brackets in (1) are calculated using the finite difference method along the dip and the strike of each of the planes. The parameter α allows for a different accuracy of the interferometry and the GPS

data: the parameter of regularization β defines the smoothness of the displacement field within each plane.

Minimization of the functional (1) is implemented on the bases of a particular modification of the Monte-Carlo method in the following way. For each component g_j of the vector **g**, the distribution type, w_j, is specified (either normal or uniform within a limited interval, depending on the physical meaning of the particular parameter), and also the initial values of expectation $a_j^{(0)}$ and variance $D_j^{(0)}$ are specified. From these values, K trial vectors $\tilde{\mathbf{g}}_k^{(0)}$ are generated (that is, K sets of nonlinear parameters of the model), with multivariate probability density $W_g^{(0)} = \prod_{j=1}^M w_j(g_j; a_j^{(0)}, D_j^{(0)})$ (the particular parameters of the model are understood as independent quantities). For each trial vector, a correspondent system of linear equations is solved, and the components of $\mathbf{u} : \tilde{\mathbf{u}}_k^{(0)}$, are found, which render the minimum of the functional (1) at the given fixed $\mathbf{g} = \tilde{\mathbf{g}}_k^{(0)}$. Then $Q < K$ trial vectors $\tilde{\mathbf{g}}_q^{(0)}$, corresponding to Q minimum values of the functional (1) at $\tilde{\mathbf{p}}_q^{(0)} = (\tilde{\mathbf{u}}_q^{(0)}, \tilde{\mathbf{g}}_q^{(0)})$ are selected.

At the next iteration, the expectations of the components of **g** are successively equated to the values of the corresponding components of the selected trial vectors: $\tilde{\mathbf{g}}_1^{(0)}, ..., \tilde{\mathbf{g}}_Q^{(0)}$, and in each case K/Q trial vectors $\tilde{\mathbf{g}}_k^{(1)}$ are generated. The type of the distribution of the component remains unchanged, and the variance is calculated by the formula $D_j^{(1)} = k_D D_j^{(0)}$, where $k_D \leq 1$ is the parameter of the algorithm. For each trial vector $\tilde{\mathbf{g}}_k^{(1)}$, an optimal vector $\tilde{\mathbf{u}}_k^{(1)}$ is determined in the way described above; Q trial vectors $\tilde{\mathbf{g}}_q^{(1)}$ corresponding to the minimum of the functional (1) are selected; and the process is repeated again. Conditions of termination may be as follows: (a) attaining the required minimum of the functional; (b) exceeding the given number of iterations; (c) reaching the state when the distance between the trial vectors (that is, the difference between the corresponding models), providing the minimum of (1) at successive iterations, becomes less than the specified accuracy of the model parameters determination.

The process of minimization is defined by three parameters: K, the number of trial vectors generated at each step; Q, the volume of the subset of vectors used as "promising" in the search for the global minimum in their vicinities, and k_D, the parameter that controls the narrowing of the search area in the course of iterations. In the numerical experiments with idealized examples, this algorithm always converged to the solution at $Q \geq K/10$ and $k_D \geq 0.5$. These are the values of the parameter that were used in solving the problem with the experimental data.

RESULTS OF THE SOLUTION OF THE INVERSE PROBLEM

Following the work [Nilssen et al., 2007], we approximated the rupture by three planes. The difficulty of the solution of the inverse problem in this case is that almost the entire set of the interferometry and geodetic data are clustered northwards of the rupture. In such conditions, the planes, approximating the rupture surface, may shift southwest to the region of the North- and South-Chuiskii Ranges. To dispose of this effect, the limits of the possible shift of the planes were fixed in such a way that the planes could not shift far from the outcrop of the seismic rupture. The rest of the parameters were free of any limitations and could vary arbitrarily.

The results of the solution of the inverse problem (1) are shown in Fig. 2. With the properly chosen parameters of smoothing and the weights of the geodetic data, we obtained a solution that is consistent with the whole data complex. The white arrows in Fig. 2 show the displacements, according to the data [Gol'din et al., 2005], and the gray arrows, the calculated displacements in the model [Nissen et al., 2007] constructed without any geodetic data. The black arrows depict the displacements calculated in our model. Because Nissen and colleagues [2007] had no GPS data available, the arrows corresponding to their solution are much shorter, and the directions of displacements in their model often disagree with the measured directions. The calculated field of LOS displacements (shown in the contours) is close to those inferred from the InSAR data (shown in shades of grey).

Our model of the rupture surface does not contradict the data of the field observations [Geodakov et al., 2003; Nissen et al., 2007]. The ruptures detected on the surface of the sedimentary cover (shown by the black dashed line in Fig. 1) agree with the positions of the planes in our model. Partitioning of any of the initial planes into smaller parts resulted in no improvement of the misfit.

The basic difference of our model against the solution by Nissen et al. [2007] is that the involvement of GPS data resulted in a considerable increase in the estimates of the displacement amplitudes on the rupture (Table 2). The authors of the cited work note that their obtained solution provides noticeably underestimated magnitudes of the seismic events, e.g., the magnitude of the main event is estimated as 6.67, against the measured one of 7.1–7.3. Our solution estimates the magnitude of the main event as 7.14, and the aftershocks, as 6.66–6.88 (Table 2), which is consistent with the seismological determinations. Another distinction between the two models considered (Fig. 2) is the different positions of the two distal planes (A and C); in our model, these planes dip more gently, compared to the model by Nissen. The parameters of the intermediate plane that corresponds to the main seismic event are rather similar in both models, although the B plane in our model dips a bit steeper, and its bottom edge lies noticeably deeper.
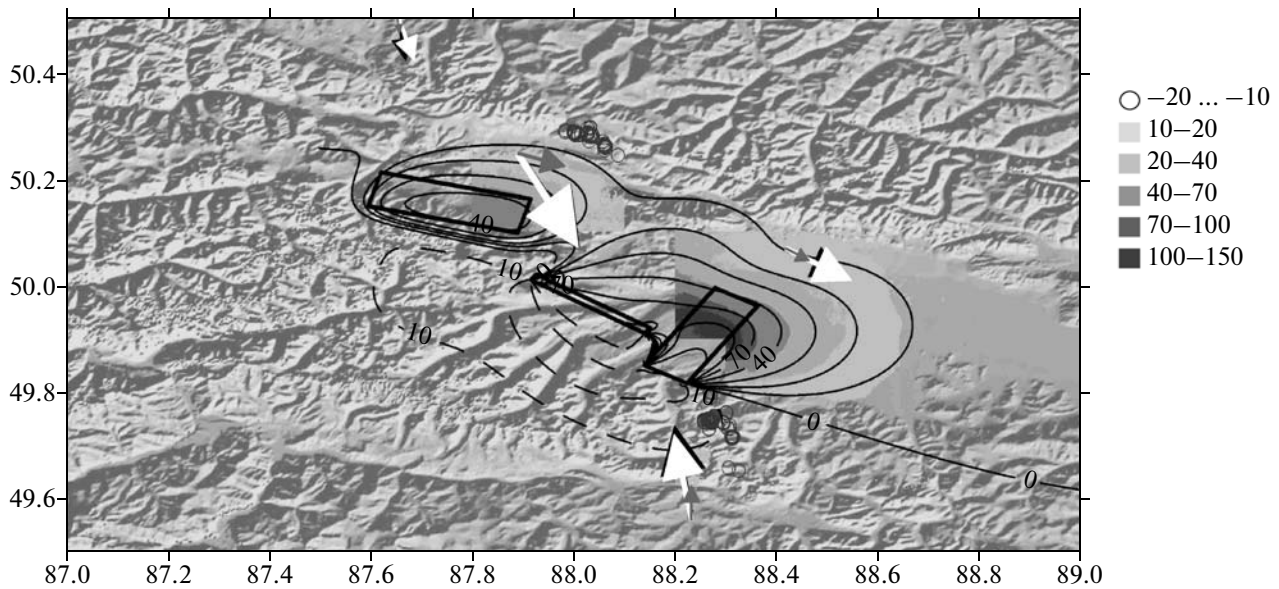
Fig. 2. Comparison of the observed and the modeled data. The observed data: the field of displacements in the LOS direction in centimeters (shown in shades of gray) calculated from the phase interferogram; the horizontal displacements (shown by the white arrows) estimated from GPS data [Gol'din et al., 2005]. Our model: the calculated LOS displacements in centimeters (shown in contours); the horizontal displacements (shown by the black arrows); the ground projection of the model rupture's surface (shown by the squares). The model by Nissen et al. [2007]: the calculated horizontal displacements are shown by the gray arrows.

The displacement on the plane *B* in our model is an almost pure shear with a very small thrust component. On the plane *C*, an almost pure thrust occurred; and on the plane *A*, both the shear and thrust components have nearly similar amplitudes.

In [Barbot et al., 2008], the surface of the rupture is strictly vertical. The displacements all over the studied region correspond to a nearly pure shear, which should result in an even stronger discrepancy with the geodetic data. Because no numerical parameters of the model were indicated in that work, no quantitative comparison has been done.

It should be noted that, despite the considerably large volume of geophysical data involved in the search for the solution, some of the rupture's parameters are determined still rather poorly. So, for the planes *A* and *C*,

nearly similar solutions exist at different depths of the upper and lower edges and at different dips of the planes. This is due to the problems of the interferogram unwrapping in regions of strong displacements and with the data clustering northwards of the rupture.

On the whole, the data available allow us to construct a rather detailed model of the rupture and to reconstruct the amplitude and the direction of displacements on this rupture. The case of the Altai earthquake is a unique event in Russia, because, in addition to the seismological and seimotectonic data, also the data of years-long geodetic observations, suitable for the detection of coseismic and postseismic events, are available for this region.

The model of displacement on the rupture shows a good agreement with the regional geodynamics. Numerous right-lateral shears are mapped during the field cam-

Table 2. Comparison of the solutions obtained from the interferometry data alone [Nissen et al., 2007] and from their combination with geodetic data (the present work)

	Plane	Strike, deg	Dip, deg	Direction of the displacement, deg	Displacement, m	Upper edge, km	Bottom edge, km	Strike length, km	Magnitude
A	[Nissen et al., 2007], Model (i)	322	80	145	1.27	1.8	25.9	12.3	6.67
B		305	80	146	1.61	0	9.7	25.3	6.77
C		295	57	96	4.63	1.4	11.4	8.2	6.76
A	This work	285	48	127	1.6	3.9	12.0	21.6	6.66
B		305	87	171	4.1	0	24.6	19.4	7.14
C		302	34	107	5.2	0	12.6	7.0	6.88

paign and the analysis of satellite images [Devyatkin et al., 1974]. The strongest earthquakes in the Altai region (e.g., the Mongolia–Altai earthquake of 1931 with $M_w = 8.0$) also had the right-lateral shear mechanisms. The shortening in this region is believed to be due to the counterclockwise rotation of a large crustal block, whose southern boundary is just that fault system where the Altai earthquake occurred [Baljinnyam et al., 1993].

ESTIMATION OF THE EFFECTS OF POSTSEISMIC PROCESSES

In the solution of the inverse problem, we used the interferometry and geodetic data that characterize different time intervals. Although this problem has been already discussed in the literature in the context of other earthquakes (see, e.g., [Peltzer et al., 1999a; 1999b; Donnellan et al., 2002]), we should admit that it is still far from being solved. To distinguish between the seismic and postseismic events is a very difficult task in our case, but it is still possible to estimate the errors that arise. Let us consider this issue in more detail.

In the solution of the inverse problem, it was implied that the available data of satellite interferometry and the geodetic data characterize the main "coseismic" events. Because, as noted above, it is impossible in our case to separate distinctly the coseismic and postseismic events, let us agree (for the purposes of discussion) to relate to the "coseismic" events, those events, which occurred since the opening of the rupture at the moment of the main shock up to the end of the rupture's northwestward propagation. It can be assumed that this period had finished with a strong aftershock on October 1, 2003 [Lutikov et al., 2003]. Even with such a duration of the coseismic processes, the available interferometry and geodetic data include both the coseismic and postseismic displacements; in addition, the proportions between the coseismic and the postseismic displacements, contained in the interferometry and geodetic data, are different. Indeed, the interferograms at hand include the postseismic events, within 12 days after the main events (after October 1, 2003) for the Kurai depression, and within almost 82 days for the Chuia depression. Repeated GPS measurements were carried out in May and June, 2004, and, hence, they include the displacements that occurred within 6–8 months after the main events. Let us attempt to estimate the possible contribution of the postseismic deformations on the basis of the available geophysical information.

Estimation of the displacements for the postseismic period from the radar interferometry data alone is a very difficult task, due to the fact that the postseismic deformations are usually small, compared to the possible atmospheric and ionospheric artifacts. Obtaining more reliable results requires several pairs of images for different periods of time, which makes it possible to dispose of noise. Among the entire set of images at hand, only the pair 7–9 (Table 1) allows identifying small displacements in the area on the plane C, within the period from

December 2003 through July 2004. In addition, the comparison of the interferograms constructed from the pair 2–10 (July 22, 2004 to September 8, 2003) with those, based on the pair 1–6 (December 6, 2003 to August 23, 2004) and the pair 2–4 (October 13, 2003 to September 8, 2003), show that in the interferogram obtained from the first pair of images, in the region of the main displacements in the Chuia and Kurai depressions, the interferometric fringes are distributed more densely, which may be indicative of a possible expansion of the displacements by one interferometric fringe (2.8 cm).

S. Barbot with colleagues [2008] used the images that were obtained 3 years after the earthquake and detected the displacements with amplitudes gradually increasing with time from 1 cm by July, 2004 to more than 3 cm by August–September, 2006. In general, a well-defined pattern of deformations in the different pairs of images, and the distinct growth in the displacement amplitudes allow us to relate these deformations to postseismic processes, because the atmospheric and ionospheric effects do not typically produce an interference pattern, persistent in time. Another important feature of the detected deformations is that they are strictly localized within a 5–10 km-wide zone around the ground projection of the upper edge of the rupture.

The cited work presents the detailed analysis of the possible mechanisms of postseismic deformations in the region of the Altai earthquake. In particular, the synthetic postseismic deformations caused by viscous-elastic relaxation of stresses produced in the lithosphere and in the upper mantle by an earthquake were calculated. Three different models of rheologic stratification of the lithosphere were considered: (1) rigid lower crust and low-viscous upper mantle; (2) low-viscous lower crust and upper mantle; and (3) low-viscous lower crust and rigid upper mantle. Compared to the interferometric data, all these models yielded deformations with noticeably larger spatial wavelengths not clustered about the rupture. The calculated deformations of the surface, associated with the fluid migration within the Earth's crust, which is driven by the variations in the pore pressure (the pore-elastic effect), also proved incapable of reproducing the observed effects. The calculated displacements, resulting from the pore-elastic deformations over the major part of the territory, have the opposite signs compared to the interferometry data. The effects, related with the postearthquake fluid migration, were observed in many regions. The absence of such deformations in the region of the Altai earthquake may be associated with the low permeability of the Earth's crust, or with the lack of a sufficient amount of the fluid within it.

Based on their analysis, S. Barbor with colleagues [2008] came to the conclusion that the observed postseismic deformations in the target region are most likely due to the postseismic creep occurring at a shallow depth along the same rupture as the main seismic event. Upon the solution of the inverse problem, they concluded that the main displacement took place at that part of the rupture, which was faintly active during the coseismic

period; the amplitude of the maximum shear at certain segments reaches 35 cm in a period of three years (in this work the whole surface of the rupture was partitioned into subregions, measuring 2×3 km).

This conclusion is indirectly confirmed by the data of GPS measurements that were carried out in 2004–2006 [Timofeev et al., 2007]. This paper does not contain any numerical data, but in the figures presented there, the orientation of the postseismic displacements through 2004–2006 is close to that of the coseismic displacements. In accordance with this work, the average rate of the displacements during 2004–2006 is 50 times lower than during the period from 2003 through 2004, which covers the main seismic events. S.V. Gol'din with colleagues [2005] estimated the accuracy of the coseismic data at the Altai geodynamical testing area as 2–3 mm per year, from which it follows that the postseismic displacements that are proceeding at a rate of 1 mm per year are close to the measurement accuracy.

In order to estimate the contribution of the postseismic displacements, let us assume that the postseismic deformations are related to the ongoing displacement on a certain surface (or surfaces) of the rupture [Barbot et al., 2008]. Let us assume also that some part of the displacements may proceed in seismic, and another part, in aseismic mode, but the proportion of these parts remains constant in time. In this case, we can estimate the rate of the decrease (in time) of the displacements, occurring on the rupture's surface and on the Earth's surface, from the decrease in seismic energy.

The difficulty of a statistically robust estimation of the average seismic energy over a finite sample is that the energy distribution of earthquakes relates to the so called heavy-tailed distributions [Pisarenko and Rodkin, 2007]. The term "heavy-tailed" means that the probability of the occurrence of an earthquake insufficiently rapidly decreases with energy. The statistical expectation of the correspondent random quantity does not exist in such distributions. In terms of mathematics, this appears as a divergence of the integral within an interval of large energies in the expectance calculation: $\langle E \rangle = \int E p(E) dE$, which is due to an insufficiently sharp decrease in the distribution density $p(E)$. In practical terms, this means that the sample mean is not a robust estimate, whose ambiguity decreases with the growth in the sample volume. A single strong event with energy exceeding the aggregate energy of all the previous earthquakes leads to a several-fold jump in the sample mean.

There are two possible ways to overcome the problem of heavy tails: the use of robust statistics for sample estimates, for instance the median values [Pisarenko and Rodkin, 2007], or the nonlinear transformation of a random value [Sadovskii and Pisarenko, 1991]. In our case, the first way is less efficient because of the insufficiently large volume of the input data. We consider the second way.

In the work [Sadovskii and Pisarenko, 1991], it is shown that, based on the data from the catalogues of earthquakes, the sample mean seismic energy of the earthquake raised to a certain power, E^{α}, can be used as a robust energy estimate for the seismic conditions in the region. The choice of the power index, α, is defined by the "energy" slope of the curve of the earthquake recurrence: the index γ contained in the energy dependence of the probability density distribution, $p \propto E^{-\gamma}$. In [Sadovskii and Pisarenko, 1991] it is advised that $\alpha < \gamma/2$. In this case, the estimate of the mean E^{α} proves to be robust (which follows, eventually, from the convergence of $\int E^{\alpha} p(E) dE$ for the expectance $\langle E^{\alpha} \rangle$). The typical values of γ range from 0.4 to 0.6, which yields the interval 0.2–0.3 for α. In [Sadovskii and Pisarenko, 1991], it is noted that the physical meaning of E^{α} is not always quite clear, but anyway this quantity may be treated as a certain tracer of the seismic energy release.

In our estimation, we shall use $\alpha = 1/3$. This value is close to the recommendations on the statistics presented above; here the quantity $E^{1/3}$ has a plain physical sense in terms of the self-similarity model of the seismic source [Abercombie et al., 2000]. Indeed, taking into account that, in accordance with this model,

$$E = \varepsilon_0 l^3; \quad \frac{E}{M_0} = k; \quad M_0 = \mu S U; \quad S = q l^2$$

(here, E is the seismic energy of the earthquake; l is its focal size; S and q are the area and the form-factor of the rupture's surface; U is the slip in the source, M_0 is the seismic moment; μ is the shear modulus; and ε_0 and k are the model constants), we obtain the expression for the slip U:

$$U = \frac{\varepsilon_0^{2/3}}{k \mu q} E^{1/3}. \tag{2}$$

Hence, in the context of the self-similarity model, the quantity $E^{1/3}$ characterizes the slip in the earthquake source. Its average value and, thus, the sum over a certain time interval are statistically robust. As an indicator, we shall use the ratio of the sum of U in (2) within the given time interval for the duration of this interval.

The input data for estimating the energy of earthquakes are taken from the seismic catalogue. We used the ISC catalogue (International Seismological Centre, http://www.isc.ac.uk, ftp://ftp.isc.ac.uk), where the basic magnitude is m_b. In [Smirnov, 2003], a detailed analysis of the magnitude scale used in the ISC catalogue is presented, and the statistical relations between the magnitude and the source parameters are derived. The latter are brought into compliance with the interrelations between the seismic moment, energy, and the source size. In accordance with the obtained relations:

$$\log E(\text{J}) = 2.71 m_{b\_\text{ISC}} - 1.81, \tag{3}$$
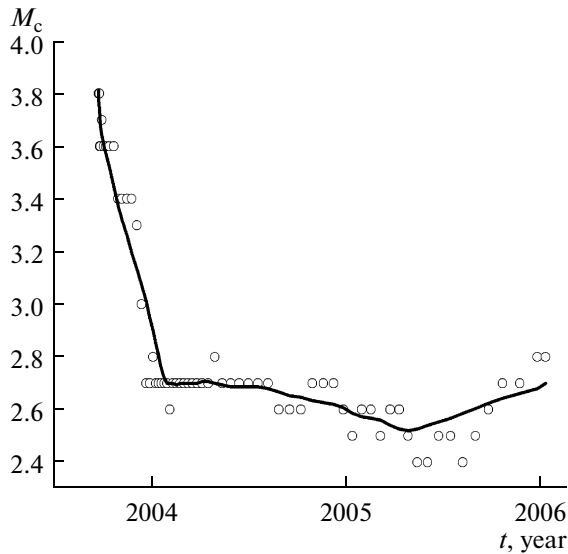
Fig. 3. Time variations in the representative magnitude, from the catalogue of aftershocks.

and the coefficients included in (2) are as follows: $\varepsilon_0 = 10^2$ J/m^3 $k = 6.2 \times 10^{-5}$, $q = 1$. These values were used in the calculations by formula (2), based on the energy estimates from (3); the value of the shear modulus was taken $\mu = 10^{11}$ Pa. The magnitude of the Altai earthquake is estimated in the ISC catalogue as $m_{b\_ISC} = 6.9$ (here, for this earthquake we presented the magnitude M_S). In accordance with the formulas (2) and (3), in this case we come to an estimate for the slip in the source of 1.5 m, which agrees with the estimates by the
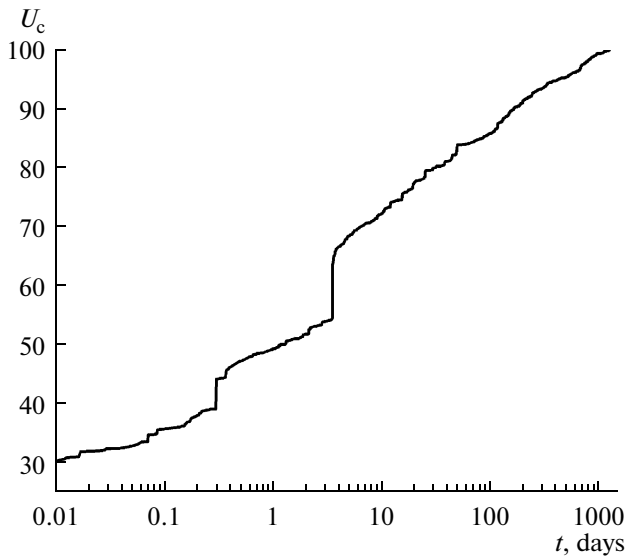
Fig. 4. Cumulative plot of $U_c(t) = \dfrac{\sum_{i(:t_i \le t)} U_i}{\sum_{\text{всe}\,i} U_i} \times 100\%$.

Time is counted from the main event.

geodetic data and thus confirms the correctness of our choice of the coefficients in (2).

The working catalogue was obtained by a formal identification of the aftershocks in the ISC catalogue. The procedure for identification was suggested in [Molchan and Dmitrieva, 1991], and its implementation is described in [Smirnov, 2009]. This catalogue included 1468 events; the size of the ellipse outlining the epicentral region of the aftershocks was 90×40 km; the azimuth of the main axis was $141°$, which agrees with the independent estimates from [Lutikov, 2003].

Figure 3 illustrates the estimation of the representative magnitude over the catalogue of aftershocks (the procedure for estimation is presented in [Smirnov, 2009]). Its time variations are typical for the series of aftershocks recorded at the regular seismic networks: the increased level of the representative magnitudes during the initial time period is associated with the overloading of the network and the system for the raw data analysis. The dynamics of the energy release since late 2003 is of major interest in the context of the present paper. The representative earthquakes for this interval are those with magnitudes $m_b \ge 2.8$, and this very value was used in the selection of the catalogue. The volume of the selected data was 1033 events.

Figure 4 depicts the cumulative plot of U_c, the aggregate value accumulated by the given time instance, expressed as the percentage of the sum over the entire catalogue:

$$U_c(t) = \frac{\sum_{i:t_i \le t} U_i}{\sum_{\text{всe}\,i} U_i} \times 100\% .$$

The data presented in Fig. 4, can be compared with the integral geodetic estimates. According to the geodetic data, the fraction of postseismic displacement (measurements three years after the main event) against the coseismic displacement (measurements within three months since the main event inclusive) is about 5%. The percentage of the postseismic to the coseismic movements in U_c within the same time interval is 6.5%. Such an agreement substantiates the possibility for the use of the seismic statistics as a marker of the intensity of the geodynamical motions.

Figure 5 displays the "release" rate of U, estimated within a running time window: $\dfrac{\Delta U}{\Delta t} = \dfrac{\sum_{i:t_b \le t_i < t_e} U_i}{t_e - t_b}$, where t_b and t_e are the beginning and the end of the window. The width of the window varies from the lesser in the beginning to the larger in the end of the series of aftershocks. This ensures the equal statistical representativeness of the estimates $\dfrac{\Delta U}{\Delta t}$. In fact, when choosing the window, we fixed the number of aftershocks that fall within the window (to be 100 events), and then we shifted the window by one event. It is seen in the figure that the
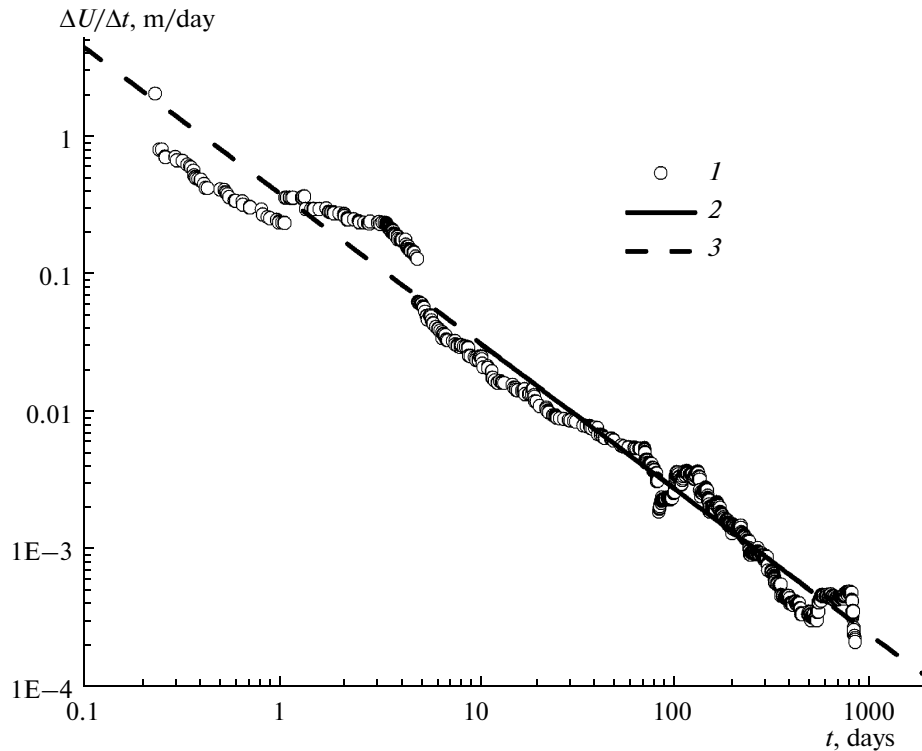
Fig. 5. The "release" rate of U. Time is counted from the main event. (*1*) is the empirical data; (*2*) is the regressive approximation within the range 10–500 days: $\log \dfrac{\Delta U}{\Delta t} = -(1.07 \pm 0.01)\log t - (0.39 \pm 0.03)$; (*3*) is the extrapolation onto the entire time interval.

decay in activity is close to obeying the power law, that is, it is consistent with the Omori law. The regressive approximation within the time interval from 10 to 500 days, which is of relevance in the context of our study, provides an estimate for the Omori law parameters: $\dfrac{\Delta U}{\Delta t} = \dfrac{10^{-(0.30 \pm 0.03)}}{t^{(1.07 \pm 0.01)}}$. The Omori's parameter, the power index of t, proved close to unity, which is typical for the aftershocks' sequences. It is apparent from the figure that the extrapolation of the obtained approximation onto the entire time interval agrees rather well with all the empirical data available.

Let us use the estimates reported in [Barbot et al., 2008] for the displacements in the nearest zone of the rupture for different time intervals. The growth in the maximum displacements, in accordance with the three postseismic interferograms presented in this work (December 22, 2003–July 19, 2004; July 19, 2004– June 19, 2006; and October 13, 2008–August 28, 2006) is approximated quite well by a hyperbolic function with the coefficient $b_i = 0.85 \pm 0.15$ cm.

Hence, we conclude that the model representing the decrease in the displacement velocity with time is consistent with the interferometric data and can be applied in the assessment of the extent of the postseismic displace-

ments within different time intervals. Using the inferred estimate, b_i, we find that since the commencement of the postseismic period (which we decided to count from October 2, 2003) up to October 13, 2003, the maximum displacement is likely to have increased by less than 1 cm, and up to December 22, 2003, by 2.4 cm. Hence, the interferometric pairs used in the estimation of the displacement, characterize mainly the coseismic events. The contribution of the postseismic events to the interferometry data for the Chuia depression (the amplitude of the displacements is about 150 cm) and the Kurai depression (the amplitude of the displacements is larger than 100 cm) does not exceed 10%.

The coefficient b_i inferred from the interferometric data cannot be applied to the geodetic data, because even if the vector of horizontal displacements, according to geodetic data, is close to the line-of-sight direction, in its projection on LOS, this vector is multiplied by the sine of the satellite elevation angle: $\sin(23°) = 0.39$ and is added by an unknown vertical displacement multiplied by $\cos(23°) = 0.92$. However, the proportion between the postseismic and coseismic displacements estimated by both methods over similar intervals of time should persist, if the direction of horizontal displacements is close to the line-of-sight (LOS) orientation. Indeed, in the situation at hand, this is the case. The coseismic displacements in the points of geodetic measurements located in the Chuia and Kurai depressions are close to the LOS direc-

tion (Fig. 1); based on the plot presented in [Timofeev et al., 2007], the postseismic displacements through 2004–2006 occurred in approximately that direction. Then, we find that the postseismic displacements in the interferometric data during the period until mid-June, 2004 were 3.3 cm maximum, that is, about 2% of the coseismic displacements in the Chuia depression, whose amplitude is more than 150 cm. Because in this case, the same proportion should be expected also for the GPS data, we conclude that the contribution of the postseismic displacements in the geodetic data reported in [Gol'din et al., 2005] may be disregarded.

Hence, our estimates of the displacements relate mainly to the processes of the rupture surface opening on September 27, 2003 and to its propagation northwestwards that proceeded up to October 1–2, 2003.

CONCLUSIONS

1. The constructed model of the Altai earthquake agrees well with the entire set of the experimental data available, including the results of the field observations and the information on the regional geodynamics. The displacements estimated in our work mainly characterize the processes that took place from the commencement of the rupture surface opening on September 27, through the end of the northwest propagation of the rupture on October 1–2, 2003.

2. In the region of the Altai earthquake, due to the dense forest vegetation and the mountain topography, the interferometric imagery characterizes the displacements mainly to the northeast of the seismic rupture, which impedes the localization of the rupture surface and the estimations of the displacement field on it. The points of geodetic measurements of the Altai geodynamical network within the nearby zone (100 km as large) are not numerous and distant from the rupture, however, the complex interpretation of the interferometric and geodetic data in these conditions provides considerably higher accuracy and stability of the solution of the inverse problem.

3. Our analysis of the contribution of the postseismic motion in the interferometric and geodetic data showed that the errors resulting from the inclusion of postseismic events into the consideration are negligibly small.

REFERENCES

1. R. Abercombie et al., *Earthquakes: Radiated Energy and the Physics of Faulting* (American Geophysical Union, Washington, DC, 2000).

2. I. Baljinnyam et al., "Ruptures of Major Earthquakes and Active Deformation in Mongolia and Its Surroundings," Geol. Soc. Am. Memoir **181**, 62 (1993).

3. S. Barbot, Y. Hamiel, and Y. Fialko, "Space Geodetic Investigation of the Co-seismic and Post-seismic Deformation Due To the 2003 Mw7.2 Altai Earthquake: Implications for the Local Lithospheric Rheology," JGR **113** (2008).

4. E. Calais, M. Vergnolle, V. San'kov, A. Lukhnev, A. Miroshnitchenko, S. Amarjargal, and J. Deverchere, "GPS Measurements of Crustal Deformation in the Baikal-Mongolia Area (1994 - 2002): Implications for Current Kinematics of Asia," JGR **108** (B10) (2003).

5. D. Cunningham, "Active Intracontinental Transpressional Mountain Building in the Mongolian Altai: Defining a New Class of Orogen," Earth Planet. Sci. Lett. **240**, 436–444 (2005).

6. D. Delvaux, K. Tenissen, R. Meer, and N. A. Berzin, "Dynamics and Paleo-Stress at the formation of the Chuia-Kurai depression in the Mountain Altai: Tectonic and Climate Control," Russian Geology and Geophysics, No. 10, 3–11 (1995).

7. E. V. Devyatkin, "Structures and Formation Units of Cenozoic Activation," in *Tectonics in the Mongolia Public Republic* (Nauka, Moscow, 1974), pp. 182–196 [in Russian].

8. A. Donnellan, J. Parker, and G. Peltzer, "Combined GPS and InSAR Models of Post-seismic Deformation from the Northridge Earthquake," Pure and Applied Geophysics **159**, 2261-2270 (2002).

9. A. R. Geodakov, A. N. Ovsyuchenko, S. G. Platonova, and E. A. Rogozhin, "Preliminary Results of Studying the Strong Earthquake of 2003 in Mountain Altai," Vestn. Otdeleniya nauk o Zemle RAN: Elektr. nauch.-inf. zhurn., No. 1 (21), 1–21 (2003) [in Russian].

10. S. V. Gol'din, V. Yu. Timofeev, and D. G. Ardyukov, "Fields of the Earth's Surface Displacement in the Chuya Earthquake Zone in Gornyi Altai," Dokl. Akad. Nauk **405** (6), 804–809]. (2005) [Dokl. Earth Sciences **405** (9), 1408–1413 (2005)].

11. R. M. Goldstein, H. Engelhardt, B. Kamp, and R. M. Frolisch, "Satellite Radar Interferometry for Monitoring Ice Sheet Motion: Application To An Antarctic Ice Stream," Science **141**, 1171–1172 (1993).

12. R. M. Goldstein, H. A. Zebker, and C. L. Werner, "Satellite Radar Interferometry: Two-Dimensional Phase Unwrapping," Radio Sci. **23** (4), 713–720 (1988).

13. Y. Fialko, M. Simons, and D. Agnew, "The Complete (3-D) Surface Displacement Field in the Epicentral Area of the 1999 M_w 7.1 Hector Mine Earthquake, Southern California, from Space Geodetic Observations," Geophys. Rev. Lett. **28**, 3063-3066 (2001).

14. J. Freymueller, N. E. King, and P. Segall, "The Co-Seismic Slip Distribution of the Landers Earthquake," Bull. Seismol. Soc. Am. **84**, 646-659 (1994).

15. R. Hanssen, *Radar Interferometry: Data Interpretation and Error Analysis* (Kluwer Academic Publishers, Dordrecht, 2001).

16. R. Hanssen and A. Feijt, "A First Quantative Evaluation of Atmospheric Effects on SAR Interferometry," in *Proceedings of the Fringe 96 Workshop, Zurich, 1996, Switzerland*.

17. K. W. Hudnut, Z. Shen, M. Murray, et al., "Co-Seismic Displacements in the Landers Sequence," Bull. Seismol. Soc. Am. **84**, 625-645 (1994).

18. S. Jonsson, H. Zebker, P. Segall, and F. Amelung, "Fault Slip Distribution of the 1999 Mw 7.1 Hector Mine, California, Earthquake, Estimated from Satellite Radar and GPS Measurements," Bull. Seismol. Soc. Am. **92**, 1377–1389 (2002).

19. A. I. Lutikov, G. Yu. Dontsova, and S. L. Yunga, "Seismological Facets of the Ms=7.3 September 27, 2003 Earthquake in the Mountain Altai: Preliminary Results," Vestn. Otdeleniya nauk o Zemle RAN: Elektr. nauch.-inf. zhurn., No. 1 (21), (2003) [in Russian].

20. D. Massonnet and K. Feigl, "Radar Interferometry and Its Application To Changes in the Earth Surface," Reviews of Geophysics **36** (4), 441 (1998).

21. D. Massonnet, M. Rossi, C. Carmona, et al., "The Displacement Field of the Landers Earthquake Mapped by Radar Interferometry," Nature **364**, 138–142 (1993).

22. G. M. Molchan and O. E. Dmitrieva, "Identification of Aftershocks: Review and New Approaches," Vychislitel'Naya Seismologiya, **24**, 19-50 (1991) [in Russian].

23. A. N. Nazaryan, *Assessment of the possibilities of SAR Interferometry in the Problems of Geoecology and Geological Hazard Assessment*, Candidate's Dissertation in Mathematics and Physics (MGU, Moscow, 2008) [in Russian].

24. E. Nissen, B. Emmerson, G. J. Funning, et al., "Combining InSAR and Seismology To Study the 2003 Siberian Altai Earthquakes-Dextral Strike-Slip and Anticlockwise Rotations in the Northern India-Eurasia Collision Zone," Geophys. J. Int. **169**, 216 (2007).

25. Y. Okada, "Surface Deformation Due To Shear and Tensile Faults in a Half-Space," BSSA **75**, 1135-1154 (1985).

26. G. Peltzer, F. Crampe, and G. King. "Evidence of Nonlinear Elasticity of the Crust from the M_w7.6 Manyi (Tibet) Earthquake," Science **286**, 272 (1998).

27. G. Peltzer, P. Rosen, and F. Rogez, "Poro-Elastic Rebound Along the Landers 1992 Earthquake Surface Rupture," JGR **103** (B12), 30131-30145 (1998).

28. V. F. Pisarenko and M. V. Rodkin, "Heavy-Tailed Distributions: Applications in the Analysis of Disasters," Vychislitel'Naya Seismologiya, **38** (2007) [in Russian].

29. M. A. Sadovskii and V. F. Pisarenko, *Seismic Process in the Block Medium* (Nauka, Moscow, 1991) [in Russian].

30. S. V. Samsonov, K. F. Tiampo, J. B. Rundle, "Application of DInSAR-GPS Optimization for Derivation of Three-Dimensional Surface Motion of the Southern California Region Along the San Andreas Fault," Computers & Geosciences **34**, 503 (2008).

31. SCIGN (Southern California Integrated GPS Network), http://www.scign.org/

32. M. Simons, Y. Fialko, and L. Rivera, "Co-seismic Deformation from the 1999 Mw7.1 Hector Mine, California, Earthquake, As Inferred from InSAR and GPS Observations," BSSA **92**, 1390-1402 (2002).

33. V. B. Smirnov, "Estimating the Duration of the Lithospheric Failure Cycle from Earthquake Catalogs," Fiz. Zemli, No. 10, 13-32 (2003).[Izvestiya, Phys. Solid Earth **39**, 794 (2003)].

34. V. B. Smirnov, "Prognostic anomalies in the seismic state: I. Methodical grounds for preparation of the input data," Geofizicheskie Issledovaniya **10** (2), 7–22 (2009) [in Russian].

35. O. E. Starovoit, L. S. Chepkunas, and I. P. Gabsatarova, "Parameters of the Altay earthquake on September, 27, 2003 on the instrumental data," Vestn. Otdeleniya nauk o Zemle RAN: Elektr. nauch.-inf. zhurn., No. 1 (21), 1-11 (2003) [in Russian].

36. V. Yu. Timofeev, D. G. Ardyukov, E. Kale, et al., "Displacement fields and models of current motion in Gorny Altai," Geol. Geofiz. **47** 8, 923–937 (2006) [Russian Geology and Geophysics **47** 8, 915–929 (2006)]

37. V. Yu. Timofeev, D. G. Ardyukov, and E. V. Boiko, "Tectonic and Post-seismic Motion in the Altai-Sayany Region according to GPS data," in *Proceedings of the III International Scientific Congress "Geo-Sibir'-2007", Novosibirsk, 2007*, Vol. 3: *Remote Sensing of the Earth and Photogrammetry, Environmental Monitoring, and Geoecology*, 274–278 (2007) [in Russian].

38. T. Tsuda, K. Heki, S. Miyazaki, et al., "GPS Meteorology Project of Japan-Exploring Frontiers of Geodesy," Earth Planets and Space **50** (10) (1998).